

Using ensemble adjustment Kalman filter to assimilate Argo profiles in a global OGCM

Xunqiang Yin · Fangli Qiao · Qi Shu

Received: 28 July 2010 / Accepted: 30 March 2011 / Published online: 20 May 2011
© The Author(s) 2011. This article is published with open access at Springerlink.com

Abstract An ensemble adjustment Kalman filter (EAKF) is used to assimilate Argo profiles of 2008 in a global version of the Modular Ocean Model version 4. Four assimilation experiments are carried out to compare with the simulation without data assimilation, which serves as the control experiment. All experiment results are compared with dataset of Global Temperature–Salinity Profile Program and satellite sea surface temperature (SST). The first experiment (Exp 1) is implemented by perturbing temperature of upper layers in the initial conditions (ICs) with an amplitude of 1.0°C and no ensemble inflation. The results from Exp 1 show that the simulated temperature (salinity) deviation in the upper 400 m (500 m) is reduced through Argo data assimilation; however, these deviations are increased in deeper layers. The error reduction in SST is much greater during January to June than during the rest of the year. Three more experiments are designed to understand the responses in different layers and months. Two of them test model sensitivities to ICs by perturbing them vertically: one over the vertical extent of the whole water column (Exp 2) and the other employs smaller

perturbation amplitude of 0.1°C (Exp 3). Exp 2 shows that the simulated temperature and salinity deviations are systematically improved in the whole water column. Comparison between Exps 2 and 3 suggests that perturbation amplitude is important. Exp 4 tests the influence of the optimal inflation factor of 5%, which is determined by other set of numerical tests. Exp 4 improves assimilation performance much more than the other three experiments without inflation. Therefore, we conclude that the perturbation should be introduced to all model layers, proper perturbation amplitude is important for Ocean data assimilation using EAKF, and the ensemble inflation by an optimal inflation is critical to improve the skill of the EAKF analysis.

Keywords EAKF · Argo profiles · Ocean data assimilation · Perturbation of the initial conditions · Ensemble inflation

1 Introduction

Ocean data assimilation (ODA) is often used to reconstruct historical time series, which can help to improve our understanding of dynamics behind ocean circulations and evolutions (e.g., Carton et al. 2000a, b; Chepurin et al. 2005; Zhang et al. 2005). ODA is also used to combine observations and numerical model to provide more accurate initial conditions (ICs) for ocean forecast. Among many ODA methods, ensemble Kalman filters (EnKF, Evensen 1994; Houtekamer and Mitchell 1998) can reveal the probability distribution of numerical models through ensemble statistic analysis. As a consequence, ensemble methods, which are maturing rapidly in recent decades, are gradually being used by many research groups for ocean prediction (e.g., Anderson 2003).

Responsible Editor: Tal Ezer

This article is part of the Topical Collection on *2nd International Workshop on Modelling the Ocean 2010*

X. Yin · F. Qiao · Q. Shu
The First Institute of Oceanography,
State Oceanic Administration,
6 Xian-Xia-Ling Road, Hi-Tech Industry Park,
Qingdao, China 266061

X. Yin · F. Qiao (✉) · Q. Shu
Key Laboratory of Marine Science and Numerical Modeling
(MASNUM), State Oceanic Administration,
Qingdao, China
e-mail: qiaofl@fio.org.cn

EnKF was originally developed to approximately compute solutions of nonlinear filtering problems by the Kalman filter (Kalman 1960; Kalman and Bucy 1961; Courtier et al. 1993). Various methods were then developed to reduce assimilation errors and/or to decrease computational cost (Anderson 2001; Bishop et al. 2001; Pham 2001; Whitaker and Hamill 2002; Tippett et al. 2003). The ensemble adjustment Kalman filter (EAKF; Anderson 2001, 2003) is one important representation of these methods. Comparing with the traditional EnKF, not only the perturbation of the observation is avoided but also the computational cost is reduced; the EAKF performs well even with moderate ensemble size (Anderson 2001; Evensen 2003; Zhang and Anderson 2003). There are many successful implementations of the EAKF method in ODA. Zhang et al. (2005) developed a parallelized ensemble filter system to assimilate the observations of 1980–2002 and compared the results with those from 3D variational data assimilation. Zhang et al. (2007) then applied the EAKF to a coupled climate model and analyzed the meridional overturning circulation from the assimilated results. Anderson et al. (2009) developed the Data Assimilation Research Testbed for data assimilation research, education, and development. This method was also used in other models, such as the El Niño/La Niña–Southern Oscillation models (Karspeck and Anderson 2007) and regional ocean models (Yin et al. 2010a).

Although the algorithm of the EAKF method is used more and more in complicated ocean models, there are still some problems that need to be studied, such as the sampling of ICs (Evensen 2004) and the inflation of ensemble samples (Anderson 2007). About the sampling of ICs, it is necessary to test the perturbation methods towards the possible states of the real ocean. In this study, numerical experiments are designed to test sensitivity from the vertical extent and the perturbation amplitude for ICs. The ensemble inflation that is performed to increase the spread of ensemble samples can be used to avoid the convergence of the ensemble members. If the probability distribution function of model states is computed using the converged ensemble members, the followed EAKF analysis will be inaccurate and unreliable. In order to obtain a proper spread, there are some attempts in the recent literature. Hamill et al. (2001) analyzed ensemble mean errors as a function of the inflation factor and noticed that the optimal inflation factor was a function of ensemble size; Anderson (2007) developed an adaptive covariance inflation algorithm using a hierarchical Bayesian approach. Zhang et al. (2010) developed an adaptively inflated ensemble filter, which employs a precomputed “climatological” variance to inflate the covariance where the ensemble would otherwise have trouble encompassing the true state. In this study, the optimal inflation factor of 5% is obtained through a series

of numerical tests. In order to maintain the intrinsic relationship among different variables, the same inflation factor is applied for all the variables in the whole model domain.

The paper is organized as follows. Section 2 describes the data used for assimilation and validation, the global ocean general circulation model (OGCM), the modular implementation of the EAKF, the designing of the experiments, and the statistic indexes used for comparison. Section 3 presents results of these experiments, including two base experiments and three sensitivity experiments for analyzing issues related to vertical extent of perturbation, perturbation amplitude, and the optimal inflation factor. Finally, summary and discussions are given in Section 4.

2 Methodology

2.1 Argo data for assimilation

The Argo profiles of temperature and salinity provided by the Coriolis Argo Data Center are employed in this study. The data are arranged by daily files in NetCDF format, which makes them easy to be used in data assimilation as input profiles by serial or parallel programs. This dataset is provided together with detailed description and quality control (QC) flags. There are two levels of QC performed on this dataset: the first level is the real-time QC that performs a set of agreed automatic checks, and the second level is the delayed-mode QC. Only those profiles passed all real-time QC tests with QC flag equal to 1 or passed the delayed-mode QC are used in our experiments. In order to deal with these profiles conveniently, two self-defined types are developed in the EAKF module: one is used to collect information for Argo temperature/salinity profiles, and the other for an observation operator to obtain modeled vertical profiles.

2.2 Data for validation

The dataset of Global Temperature-Salinity Program (GTSP) provided by the US National Oceanographic Data Center is used in this study for validation. Most of the Argo profiles are contained in the dataset of the GTSP but they are removed from the GTSP before we perform validation (hereafter, we use GTSP presents those profiles in GTSP dataset eliminated Argo profiles). The modeled results are interpolated onto the same location as the GTSP profiles for a more accurate comparison.

The statistical information for Argo and GTSP profiles is given in Fig. 1. It is clear that most regions of the global ocean could be covered by both Argo profiles and GTSP profiles and the observing network of Argo is much better

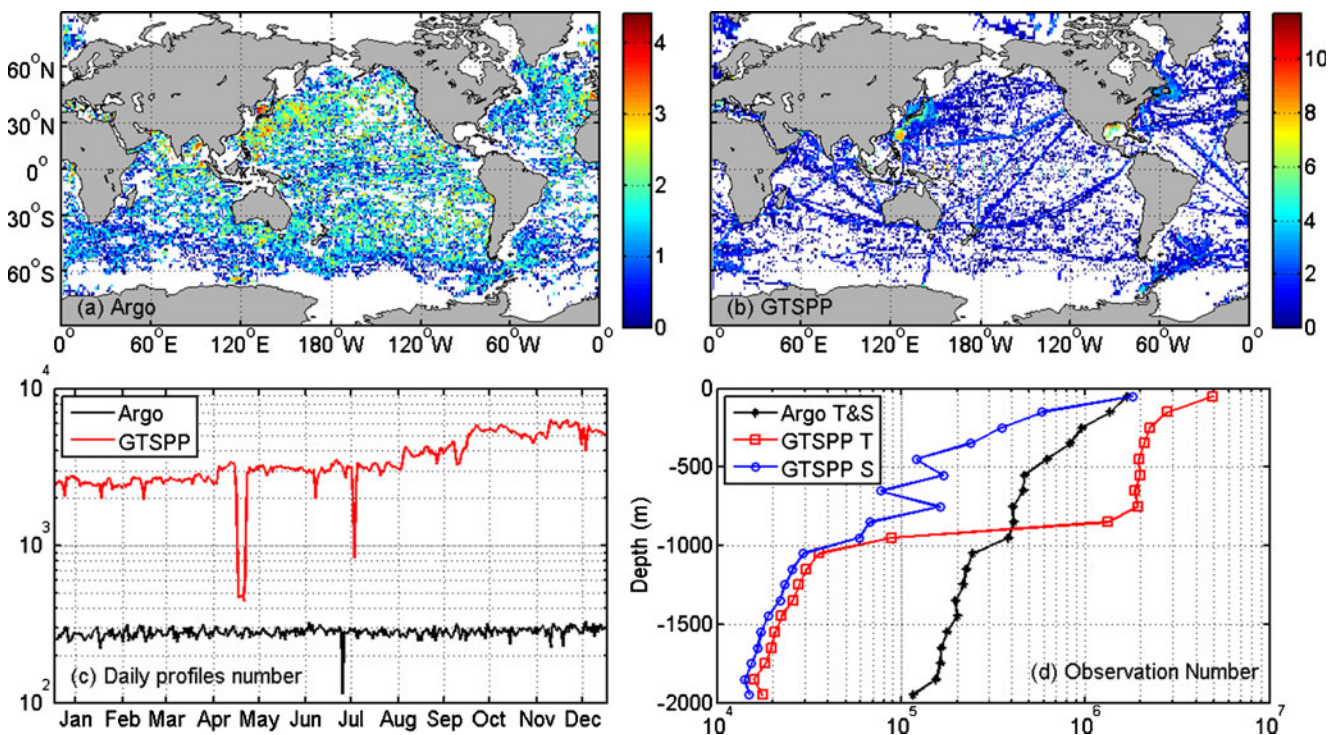


Fig. 1 The statistical information of GTSP and Argo profiles in 2008. **a** The distributions of Argo profiles with the color presents the logarithm of the profile number at the $1^\circ \times 1^\circ$ boxes; **b** same as panel **a** but for GTSP; **c** the daily profile numbers for Argo and GTSP; **d**

the observation (temperature and salinity) numbers of Argo and GTSP at each 100 m-layers. Here, GTSP presents those profiles in GTSP dataset eliminated Argo profiles

than that of GTSP. However, both the GTSP daily profile numbers and the total GTSP profile numbers counted in each horizontal $1^\circ \times 1^\circ$ grids are much larger than those of Argo. Each Argo profile contains temperature and salinity observations together, but some GTSP profile may only contain temperature or salinity observations. Compared to the observations in Argo, the number of GTSP temperature observations is larger in the layers upper than 1,000 m, but it is smaller in the deeper layers. For the observation of salinity, the numbers in GTSP are smaller than in Argo at all depth. Therefore, GTSP profiles used as an independent dataset can provide enough observations to evaluate the model performance before and after Argo assimilation, and make it possible to do statistical analysis for the 3D structure of errors.

The satellite sea surface temperature (SST) used for comparison is the optimally interpolated microwave (MW) SST product created from the SSTs of two satellites: the MW Tropical Rainfall Measuring Mission Microwave Imager (TMI) and the Advanced Microwave Scanning Radiometer–Earth Observing System. This dataset is produced by the Remote Sensing Systems and sponsored by the National Oceanographic Partnership Program, the National Aeronautics and Space Administration (NASA) Earth Science Physical Oceanography Program, and the NASA Measures Discover Project, which is available at

www.remss.com. It is an improved version of SSTs from multisensors, and provides daily average globally with a horizontal resolution of $0.25^\circ \times 0.25^\circ$. Extensive comparisons are provided at that website, and the statistics shows that these SSTs have a standard deviation equal to 0.56°C for collocations within the range of the TMI data (40°S – 40°N), while a higher one equal to 0.65°C for the global collocations (90°S – 90°N). Similar as dealing with the GTSP profiles, the model outputs of all experiments are interpolated onto the same grid as the satellite SST before comparison.

2.3 A global OGCM based on MOM4

The Modular Ocean Model version 4 (MOM4; Griffies et al. 2007) is used to setup a global coupled ice-ocean model. The surface wave-induced vertical mixing is included into the model based on Qiao’s parameterization (Qiao et al. 2004). The model domain is 81.5°S – 89.5°N around the globe, and the horizontal resolution is $1^\circ \times 1^\circ$ everywhere except for the tropical ocean (30°S – 30°N) where the resolution is $(1/3)^\circ$ in the meridional direction. There are 50 vertical levels, with 10-m resolution for the top 220 m and reduced resolutions below. The model topography is interpolated from a gridded bathymetric dataset of $5' \times 5'$ resolution (ETOP5 1986) with the maximum depth set to

5,500 m. As a component of MOM4, Sea Ice Simulator is a dynamics/thermodynamic sea ice model that employs a three-layer scheme for the thermodynamics and full dynamics with internal ice forces calculated using elastic-viscous-plastic rheology (Winton 2000).

The model uses the annual mean temperature and salinity from Levitus and Boyer (1994) as its ICs, and is driven by climatological atmosphere forcing from the Ocean Model Intercomparison Project (OMIP; WOCE/CLIVAR 2002). The model state after 11 years of spin-up is taken as the ICs for the year of 2000 for simulation with surface forcing from the National Centers for Environmental Prediction reanalysis data (Kalnay et al. 1996) provided by the NOAA/OAR/ESRL PSD, Boulder, Colorado, USA, including wind, atmosphere temperature and sea level pressure. The rest of the forcing is from the climatological dataset of OMIP. More details, including validation of this model, can be found in Shu et al. (2011).

2.4 An EAKF module for Argo profiles

The assimilation system used here is composed of two main parts: the ensemble members and the EAKF module. The ensemble members, which are the integrations of the same model from different perturbed ICs, are running separately. At beginning, the EAKF module will be started first to collect the information of observations (include the observed time, location, and values), then send message to each ensemble members about the observing time, and waiting for the predicted ensemble states. All the ensemble members will start the model integration together to predict the ensemble states of the ocean. Once the predicted ensemble states at observing time are available, the EAKF module will receive these data and start the EAKF analysis to update the ensemble states by EAKF. The updated results will be sent back to each ensemble members and the ensemble integration will be continued for the next observing time.

The parallelization strategy of each ensemble member is based on its original design and arranged as an ensemble (Fig. 2a). A module is designed for the EAKF analysis by parallel. In this module, the computing domain is divided into several blocks with a region called “halo” for overload computing as shown in Fig. 2b. The “halo” region should be big enough to ensure the results from parallel computing are identical to those from serial computing. In this study, three times of the horizontal scale for covariance localization is used as the “halo” size. In Fig. 1b, *myis* (*myie*) and *myjs* (*myje*) are the start (end) grid indexes of this block, and the related longitude and latitude are *islon* (*ielon*) and *jlat* (*jelat*), respectively. The region for a spatial block is *myim* by *myjm* and the efficient computational region is *ielon-islon* by *jelat-jlat* or *myie-myis* by *myje-myjs*.

The whole system including ensemble members and EAKF module can be arranged by UNIX shell scripts or parallel languages such as MPI, OpenMP, etc. If the assimilation frequency is not too high, say once every day, it is more efficient to arrange the system by scripts with required information exchanged through input/output files. Consequently, it will be more portable for the EAKF module to other ocean models from the MOM4 used here; what is all needed is to write some general procedures to deal with variables from different models. If the assimilation frequency is very high, it is necessary to combine the EAKF process with the ensemble members in order to exchange information faster. In most cases, the observation frequency is not so high. Therefore, arranging the system by scripts is an efficient choice.

The EAKF module specified here is for assimilating the Argo temperature and salinity profiles. During the process of the Argo profiles being assimilated into the ocean model, the EAKF is performed for multivariables. In other words, once the Argo temperature profiles are used to adjust model temperature, the model salinity is also adjusted by the covariance between salinity and temperature. On the other hand, a similar procedure is performed for the Argo salinity profiles. The standard deviations of errors for observed temperature and salinity in this study are chosen to be 1°C and 0.2 psu, respectively. The localization of covariance is performed by a polynomial function, same as in Zhang et al. (2005), and the Euclidean spatial distance in this function is selected as 2° horizontally, 100 m vertically and 5 days in time.

2.5 Experiment design

2.5.1 Base experiments (CTL and Exp 1)

The year of 2008 is the focus period of this study and the model simulation without the ODA is referred as the control run (CTL). The ICs of the ensemble members are prepared from CTL. The method for generating random fields given by Evensen (1994) is used here to perturb the surface fields and then the surface perturbations are smoothly projected to subsurface layers. The random fields are smooth spatially, and their spatial correlation decreases with increasing distance. Therefore, this kind of perturbation will not break the smoothness of the integration itself.

Based on the previous studies (Mellor and Ezer 1991; Ezer and Mellor 1994, 1997; Yin et al. 2010b), the information at surface can be projected into the deep ocean. Inspired by these works, new methods are designed using a simple way instead of statistically computing the correlation factors. The new vertical projection carried out in this study is to project the surface perturbation into subsurface layers. Since the upper ocean is often much more variable

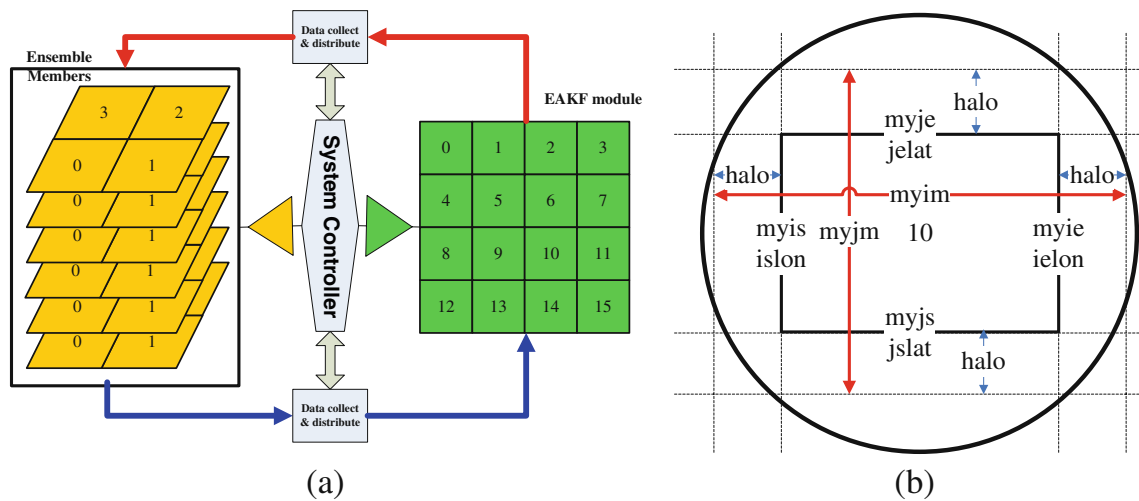


Fig. 2 System design of the EAKF module: **a** structure of assimilation system, and **b** parallel design for the EAKF module

than the deeper ocean, the projection used in the first assimilation experiment (Exp 1) is mainly performed for the upper mixed layer with few additional layers below for relaxing the perturbation to 0 in the deeper part of the ocean. The detailed projection method can be described as follows.

$$T_{ij,k,n}^p = \begin{cases} T_{ij,k} + CP_{ij,n} \left(1 - \frac{T_{ij,1} - T_{ij,k}}{\Delta T}\right), & k \leq k_1 \\ T_{ij,k} + CP_{ij,n} \left(1 - \frac{T_{ij,1} - T_{ij,k_1}}{\Delta T}\right) \left(1 - \frac{k-k_1}{kk}\right), & k_1 < k \leq k_1 + kk \\ T_{ij,k'} & k > k_1 + kk \end{cases} \quad (1)$$

where P is the generated random fields; T_k is the temperature before perturbation; subscripts i and j are grid indexes on horizontal space; subscript k is for model layer index; subscript $n = 1, \dots, N$ is the ensemble index where N is ensemble size and equal to 8 in this study; superscript p means perturbed value; ΔT , which represents temperature difference between surface and the bottom of the mixed layer, is set to 1°C in this study; k_1 is the layer index for the bottom of the mixed layer and defined as the first layer whose temperature has 1°C difference from the surface; kk is the number of relaxing layers; and C is a parameter used to control perturbation amplitude. The absolute operator in Eq. 1 ensures that the perturbation below the surface will never be greater than the perturbation at surface.

In Eq. 1, the vertical layers are divided into three parts: the first part is for the upper mixed layer with the perturbations of CP at surface and 0 at the bottom of the upper mixed layer; the second part includes layers whose perturbations are smoothly reduced to 0 from the perturbation in the layer of k_1 , in case the bottom of the upper mixed layer is not exactly located at vertical model grids; and the third part is for the remaining layers that are kept unperturbed. The second part is chosen to be five layers or less, which could include the bottom layer if the third part has zero layer.

In order to simplify the perturbation of ICs, only the temperature field is perturbed for the ensemble members. The perturbations are normalized by C to ensure the root mean square (RMS) of surface perturbation equals to a specific value defined as the perturbation amplitude. For Exp 1, the perturbation amplitude is 1°C . Accordingly, the perturbed layers in Exp 1 are limited to the upper layers of the ocean, and in general they are only few hundred meters below the sea surface.

2.5.2 Sensitivity experiments (Exps 2–4)

In addition to the base experiments, we carry out three sensitivity experiments to understand the roles of perturbed layers (Exp 2), perturbation amplitude (Exp 3), and the ensemble inflation (Exp 4). These assimilation experiments and their settings are listed in Table 1.

As will be discussed in the following sections, only perturbing the upper layers of the ocean is not enough to obtain a reliable spread of ensemble members. So another projection method is designed by considering of perturbing the whole water column. In this new method, despite the new perturbation is performed for the whole water column, we change the reference layers to those with maximum temperature difference from the surface. Then the projected perturbations for all layers are linearly changed according

Table 1 List of assimilation experiments

Experiment name	Perturbing layers	Perturbation amplitude	Inflation factor (%)
Exp 1	Upper	1.0	0
Exp 2	All	1.0	0
Exp 3	All	0.1	0
Exp 4	All	1.0	5

to the maximum temperature difference. This perturbation method can be described by Eq. 2 and is being used in Exps 2–4.

$$T_{i,j,k}^p = T_{i,j,k} + CP_{i,j,n} \left(1 - \left| \frac{T_{i,j,1} - T_{i,j,k}}{\Delta T_{i,j}} \right| \right), \quad (2)$$

where, $\Delta T_{i,j}$ is the maximum temperature difference of the whole water column from its surface, and the other symbols are the same as those in Eq. 1.

In this way, if the temperature in a special layer has the maximum difference with the surface temperature, its perturbation will be zero. For most cases, the bottom of the whole water column has the maximum temperature difference with the surface, and then the perturbation in the bottom layer will be zero. In general, the deeper part of the ocean has smaller perturbation.

This perturbation method is used to perturb the initial temperature fields for the sensitivity experiments. The sensitivity of perturbation amplitude is also tested by setting the perturbation amplitude equal to 1.0°C and 0.1°C in Exps 2 and 3, respectively.

The last experiment (Exp 4) is employed to test the ensemble inflation, which can avoid the convergence of ensemble samples. The inflation used here can be expressed by the following equation.

$$X_n = \bar{X} + \left(1 + \frac{\beta}{100} \right) (X_n - \bar{X}), \quad (3)$$

where, X_n is the n th ensemble member, the overbar means the ensemble mean, and β is the inflation factor that indicates how many percent the ensemble samples are inflated.

The inflation factor used here is the same for all the model variables and kept constant spatially. In this way, the relationship between different variables, or between different locations for the same variable, is not changed by the ensemble inflation. The adjustment of multivariables can be performed correctly with a better representation from a broad ensemble spread. However, the inflation factor needs to be determined beforehand. Here, a series of numerical tests are carried out to determine the optimal inflation factor. Different from the method used by Hamill et al. (2001), the inflation in this study is only performed when the amplitude of the ensemble spread at surface becomes smaller than the initial value, say 1°C in temperature. The inflation factor is changed from 0% to 10% by 1% and the RMS errors in temperature are compared in Fig. 3 for different layers covering 0–1,000, 1,000–2,000, and 0–2,000 m. The result shows a minimum value where the inflation factor is around 4–6%. So 5% is chosen as the optimum inflation factor for Exp 4. The difficulties in determining the optimal inflation factor are computation and storage costs.

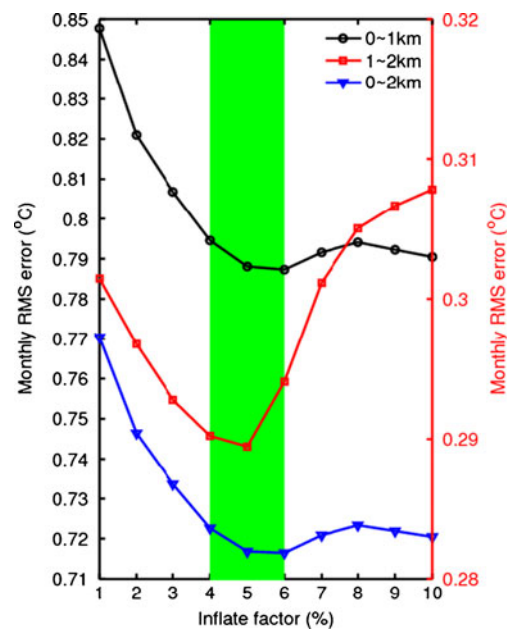


Fig. 3 Monthly mean RMS temperature errors as a function of inflation factor. The right y-axis is for the temperature error at the depth 1,000–2,000 m. A set of numerical tests, which assimilated Argo profiles for the first month in 2008 with different inflation factors, are carried out to determine the optimal inflation factor. The inflation factor changed from 0% to 10% by 1% and the RMS error of temperature showed a minimal value where the inflation factor is 4–6% (shaded)

2.6 Statistic indexes for comparison

RMS error is employed to measure the difference between observations and the results from our numerical experiments. In order to compare daily mean satellite SST and GTSP profiles exactly, the model output is saved as daily average. For the GTSP profiles, RMS errors in temperature and salinity are computed in different layers with the layer thickness set to be 100 m. The RMS errors for the whole year of 2008 are computed first, and then the RMS errors on each day are computed. For satellite SST, two kinds of RMS error are computed in this study: one is temporal RMS error obtained over the spatial SST array at the same time, and the other is spatial RMS error that is computed from the time series at the same grid point.

An assimilation index (AI) is used to analyze the assimilation performance relative to CTL.

$$AI = \frac{RMSE(CTL) - RMSE(EAKF)}{RMSE(CTL)} \times 100, \quad (4)$$

where, RMSE(CTL) is the RMS error in CTL and RMSE(EAKF) is the RMS error after Argo data assimilation. The RMS error is the measurement of the distance between simulated results (CTL or after Argo assimilation using EAKF) and the observations. The meaning of AI is the percentage error reduction, which can provide a clear view

focused on the difference due to the ODA. And the more AI achieved the more confident in the ODA.

3 Analysis of assimilation results

3.1 Comparison with the GTSP profiles

The RSM errors in temperature and salinity for all experiments are shown in Fig. 4, which are obtained over the study period of 2008 at each depth. As the reference for assimilation experiments, the results of CTL are first compared with the GTSP temperature and salinity profiles. For temperature errors, the maximum value is located at the depth near 150 m, and the error decreases quickly between 150 and 1,000 m. The simulated temperature error below 1,000 m is quite small. Since the vertical gradient of temperature around the depth of the upper ocean mixed layer is quite large, the error of this depth will be enlarged in the comparison of temperature. The maximum errors in temperature occurred at subsurface indicates that there should be some errors in the depth of upper ocean mixed layer in CTL. The salinity error shows similar distribution except that the maximum error is located at surface. The maximum salinity error at surface is caused by the use of climatological evaporation and precipitation.

In Exp 1, the RMS error in temperature (salinity) after Argo data assimilation is reduced in the layers shallower than 400 m (500 m). However, both temperature and salinity errors in Exp 1 are increased in the deeper part of the ocean. This indicates that only perturbing upper layers of the ocean may lead to an inaccurate EAKF analysis in the deeper part of the ocean.

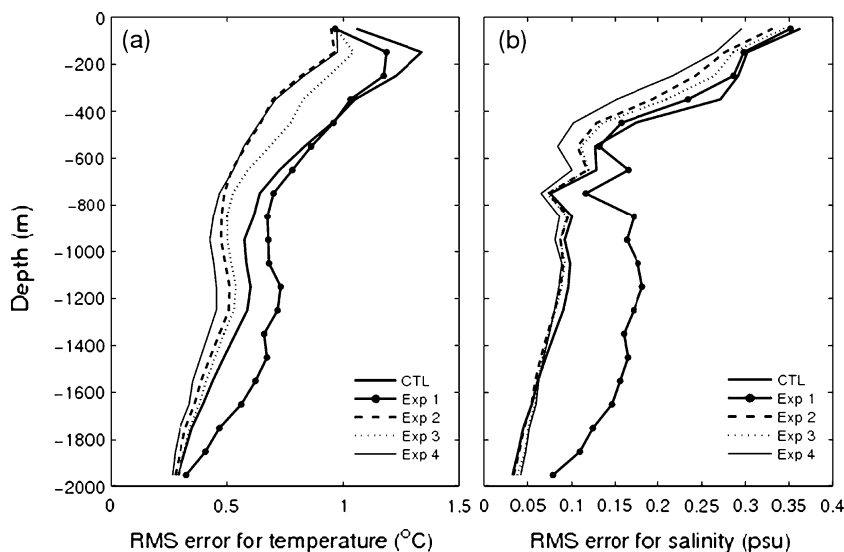
To understand and solve the problem seen in Exp 1, we carried two sensitivity experiments to check if the ODA

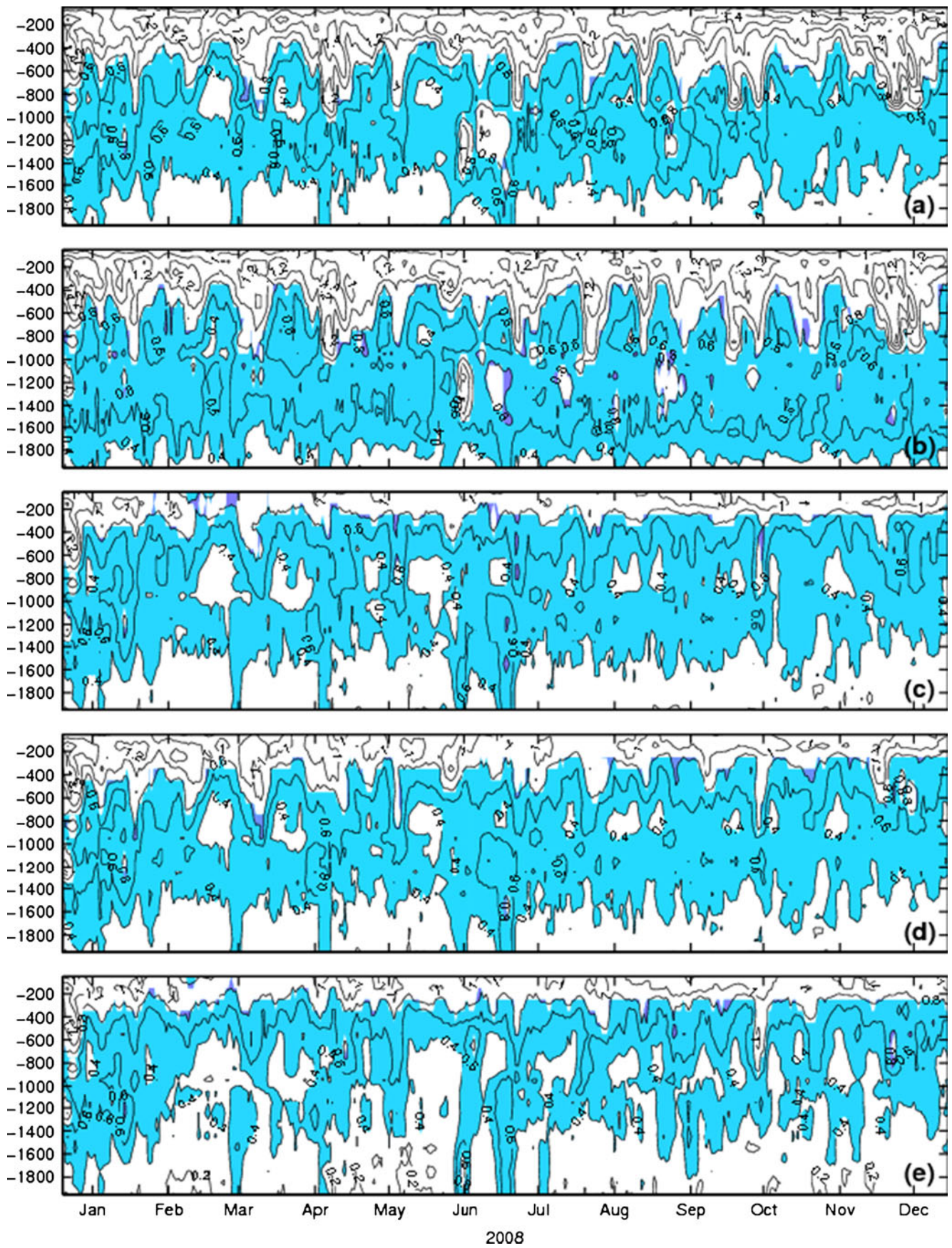
performance could be improved by perturbing the ICs with different vertical extent or amplitude. In Exp 2, the temperature of ICs is perturbed in all layers of the water column. As a consequence, the RMS errors in temperature and salinity compared with the GTSP profiles are systemically reduced in all layers. Comparing the results from Exps 2 and 3, when the perturbation amplitude changes from 1.0°C to 0.1°C, we find that smaller perturbation amplitude will degrade the ODA performance.

Recall that there is 5% ensemble inflation applied in Exp 4 to increase the ensemble spread, the vertical RMS errors of temperature and salinity from Exp 4 show that it has the best results among all the experiments. In the layers shallower than 700 m, the temperature error in Exp 4 is comparable to that in Exp 2, whereas the simulated salinity error is much reduced after including the ensemble inflation. In the layers deeper than 700 m, the simulated temperature error is reduced more in Exp 4 than in Exp 2. For salinity, the errors for Exps 2 and 4 are quite similar in the layers deeper than 1,000 m where the salinity errors are already quite small.

Detailed vertical and temporal distributions of RMS error in temperature are given in Fig. 5. The distribution from CTL shows that there clearly exists a subsurface region where the temperature errors are even larger than 1.2°C. For the layers deeper than 1,500 m, the temperature errors are less than 0.4°C most of the time. Regions with temperature RMS errors between 0.4 and 0.8°C (shaded) cover more than half of the water column in the top 2,000 m. The result of Exp 1 (Fig. 5b) shows that the RMS error is reduced in the upper layer where the temperature errors are greater in CTL. However, the shaded region between 0.4 and 0.8°C becomes larger and extends deeper in Exp 1, which means the temperature error increases in the deeper layer of the ocean. The distribution from Exp 2

Fig. 4 RMS error in **a** temperature and **b** salinity at different depth. In Exp 1, the RMS errors in temperature and salinity are reduced in the layers shallower than 500 m, while those errors in the deeper part of the ocean are increased. Once the whole column of the ocean is perturbed in Exps 2–4, the temperature errors are reduced systemically. For changing due to different perturbation amplitude, the RMS error is smaller in Exp 2 than in Exp 3. The ensemble inflation further enhances the error reduction in temperature and salinity





◀ **Fig. 5** Temporal and vertical distributions of the RMS error in temperature: **a** CTL, **b** Exp 1, **c** Exp 2, **d** Exp 3, and **e** Exp 4. The contour interval is 0.2°C and the regions where the temperature error is between 0.4 and 0.8°C are shaded to clearly show the differences among these experiments

(Fig. 5c) shows that the temperature errors for all layers in the upper 2,000 m decrease after the perturbation of ICs performed for the whole water column. The comparison between Exps 1 and 2 shows that the error reduction at surface is greater in Exp 2 than in Exp 1. This difference indicates that perturbing all layers can improve the ODA performance in the whole water column. For sensitivity to perturbation amplitude (Exps 2 and 3), although the difference at surface is greater at the beginning of the Argo data assimilation, it is not quite obvious for the rest integration time. The result from Exp 4 (Fig. 5e) shows the smallest errors among all the experiments. The shaded region in Exp 4 becomes much smaller than that in Exp 2, and the bottom of this region moves upward. This indicates that the RMS error in temperature is much reduced after including an optimal inflation factor of 5%.

Similar results are obtained from the vertical and temporal distributions of salinity RMS error. The detailed error structure in salinity from CTL (Fig. 6a) shows that the maximum salinity error (up to 0.7 psu) appears near 250 m during February–April 2008. For the layers deeper than 1,000 m, the salinity errors are generally less than 0.1 psu though values between 0.1 and 0.2 psu exist. The result of Exp 1 (Fig. 6b) shows an improvement at surface, but the salinity error increases in the subsurface region of the ocean and the shaded region in Exp 1 becomes larger and extends deeper than that in CTL. After the perturbation is applied to the whole water column in Exp 2, the salinity RMS errors are systemically reduced after the ODA (Fig. 6c). Comparison of Fig. 5c–d shows that the salinity RMS error in Exp 2 is reduced a little more than that in Exp 3 (Fig. 6d). Compared with Exp 3, the salinity error in Exp 4 (Fig. 6e) is systemically smaller than that in Exp 2. Especially in the layers deeper than 800 m, the salinity error in Exp 4 is significantly reduced by introducing the optimal ensemble inflation.

Since only the temperature fields were perturbed in ICs, the ensemble spread of salinity is generated because of the model integration itself. The variance of salinity is relatively smaller which caused the ensemble spread of salinity is not large enough to provide an accurate filtering. On the other hand, the variance of temperature in deep layers is smaller than upper layers. This also caused the smaller ensemble spread in deep layers. As a result, the ensemble inflation works well on salinity in upper layers and on temperature in deeper layers. It is indicated that the inflation benefits to those part where the ensemble spread is small.

Overall, the assimilation results are improved because of the perturbation in all layers and the perturbation amplitude is important for the error reduction at the beginning period of the ODA. Ensemble inflation is critical to improve the skill of the EAKF analysis.

3.2 Comparison with satellite SST

Since satellite SST data has a good spatial and temporal coverage of the world ocean, the comparison between modeled and satellite SSTs can provide some insight to the spatial and temporal evolution of simulation error.

The temporal SST error in CTL (the thin line in Fig. 7a) is smaller in the period during April–May 2008 and the maximum error is around the end of August. In Fig. 6a, the red thick line is for ensemble mean and the green shaded region means the range of RMS errors for all the ensemble members. It shows that the RMS errors are well reduced during January–June 2008; however, the reduction is not obvious in the second half of 2008 and the shaded region is reduced in time. These results indicate that the spread of the ensemble models is convergent along the model integration of Exp 1.

The AI is shown in Fig. 7b, which represents the percentage reduction of RMS error by ODA. The comparison between Exps 2 and 3 shows that the perturbation amplitude is important for the beginning period of ODA, but not so for the later period. Once the model state is perturbed, the model will adjust according to model physics to reach a new balanced state during the beginning period. If the perturbation is very small, this period of adjustment will be very short. This is the reason why the AI increases gradually in Exp 3 while it jumps quickly to a high level at the beginning of Exps 1 and 2. The perturbations in the deep layers of the model ocean will remain for a long time because the variance in the deep layers is not intensive. Although the perturbation at the beginning is relatively small in Exp 3, the growing mode of model errors would increase the ensemble spread at the later period of integration (Yin and Oey 2007) and thus improve the performance of Exp 3 in the last few months. After the ensemble inflation is applied in Exp 4, the AI is increased and kept the highest value during all the ODA period.

The spatial SST RMS error for CTL is given in Fig. 8a, with the regions shaded by colors to show where the SST error is greater than 1°C . The most shaded regions in CTL include the northwestern Pacific Ocean, the northwestern Atlantic Ocean, and the southern parts of the Indian Ocean, the Pacific Ocean and the Atlantic Ocean. The SST errors for the rest part of the world ocean are mostly less than 1.0°C . In Exp 1 (Fig. 8b), the shaded regions become smaller and the high errors in SST are reduced after the ODA. In the coastal regions, the error

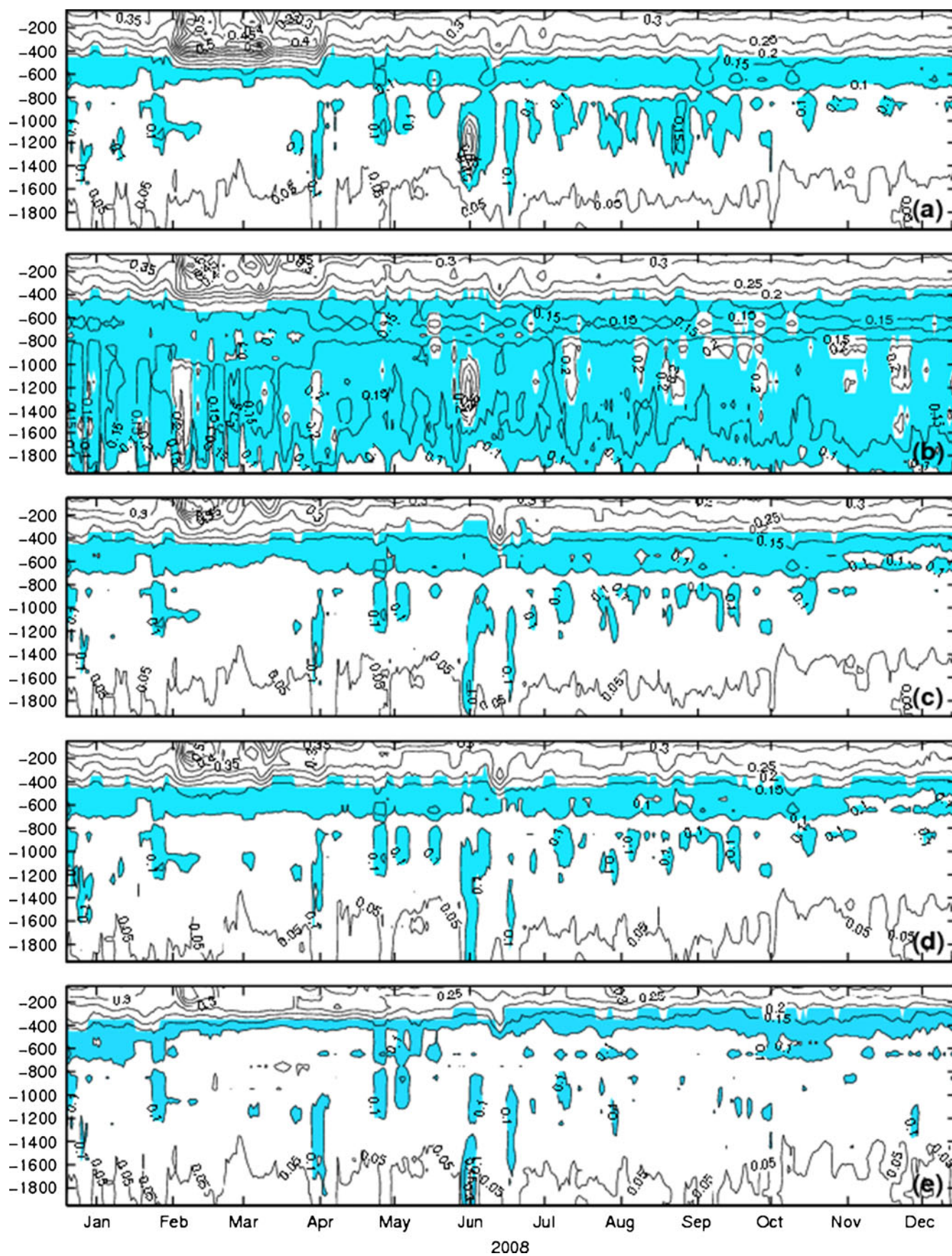


Fig. 6 Temporal and vertical distributions of the RMS error in salinity: **a** CTL, **b** Exp 1, **c** Exp 2, **d** Exp 3, and **e** Exp 4. The contour interval is 0.05 psu and the regions where the salinity error is between 0.1 and 0.2 psu are shaded to clearly show the differences among these experiments

reductions are small because of the lack of Argo profiles for ODA. The big errors in CTL are also occurred at the regions of the Extensions of Kuroshio and Gulf Streams because the activity of eddies in these regions is quite sensitive which are hard to be solved by the grid system of this model. That is why the errors in these regions are still big after ODA.

In order to clearly show the improvement of the ODA, the percentage error reduction in SST is given in Fig. 8c for Exp 1. Since AI presents a relative error reduction, the similar AI at different regions means different absolute

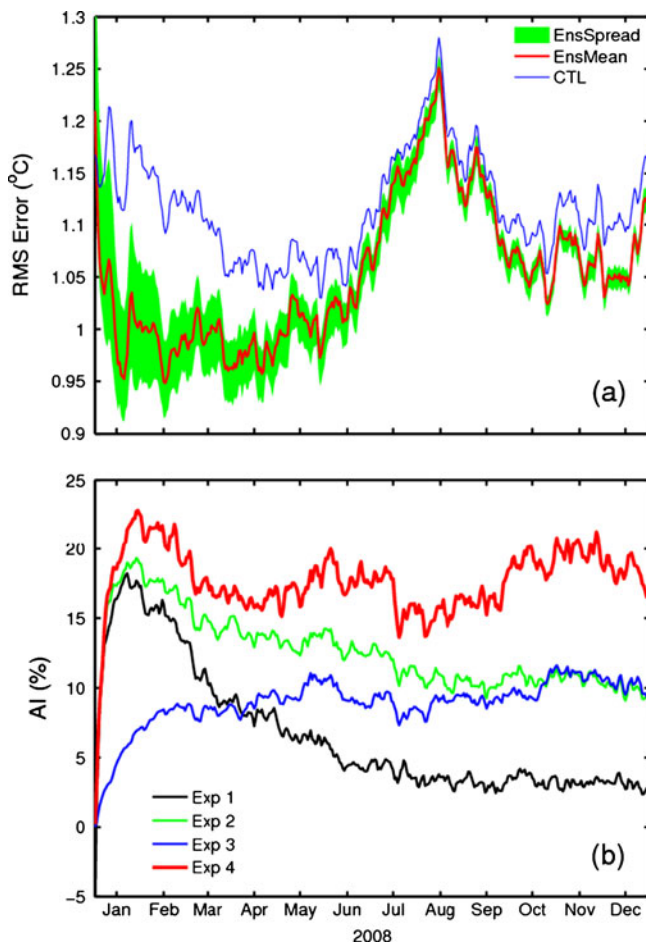


Fig. 7 Temporal **a** SST RMS errors and **b** the AI for assimilation experiments. The *thin line* is for CTL, *thick line* is for the ensemble mean in Exp 1, and the *shaded regions* are for the range of the RMS errors of ensemble samples in Exp 1. AI is defined as the percentage error reduction relative to CTL and used to show the improvement after the ODA. The reduction of SST RMS error in Exp 1 during January–June 2008 is larger than in the rest of the year. The *shaded region* indicated the ensemble samples become convergence along model integration

error reduction. This distribution shows that SST error is reduced in most regions with a positive AI. However, the SST error in some regions is not reduced (AI equals to zero) or increased (negative AI), such as the equatorial region of the Atlantic Ocean.

Figure 9 shows the percentage reductions of SST error for Exps 2–4. The AI of Exp 2 (Fig. 9a) is increased in most regions, meaning that the SST error is reduced after the perturbation performed for all layers of the ocean. The result in Exp 3 with smaller perturbation amplitude becomes worse, and the AI in Fig. 9b even becomes negative in the equatorial region and some regions of the Southern Ocean. In addition, there also exist some regions in Exp 3 where the AI is increased, such as the northwestern Pacific Ocean. Further studies should be carried out to test whether the perturbation amplitude should have a non-uniform spatial structure. As shown in Fig. 9c, the improvement due to the ensemble inflation occurs in most regions of the model domain.

These comparisons with satellite SST suggest that the perturbation should be introduced to all model layers, proper perturbation amplitude is important for ODA using EAKF, and the ensemble inflation by an optimal inflation factor can improve the performance of Argo data assimilation.

4 Summary and discussions

An EAKF module is designed for parallel computing by splitting the model domain into several blocks with overload computing regions. The associated EAKF system is arranged for separate computing with information exchanged through input/output files. The EAKF module is used in a global OGCM based on MOM4 to assimilate Argo profiles (both temperature and salinity) in 2008. Five experiments are carried out, which include the CTL that has no ODA, Exp 1 in which the perturbation of ICs is only performed for the ocean upper layers, Exps 2 and 3 by which the number of layers and the amplitude are tested for the perturbation of ICs, and Exp 4 that examines the ensemble inflation with an optimal inflation factor.

The comparisons of model results and GTSP profiles (Figs. 4, 5, and 6) show that the temperature and salinity RMS errors are reduced in the layers shallower than 500 m after Argo data assimilation. In the layers deeper than 500 m, however, the results in Exp 1 become worse than CTL. This indicates that only perturbing upper layers of the ocean is not enough. Once all layers of the water column are perturbed in Exps 2–4, the temperature and salinity errors are systemically reduced comparing with CTL. The comparisons in vertical and temporal show that perturbation of all layers can improve the results not only in the deeper part but also in the upper part of the ocean. The

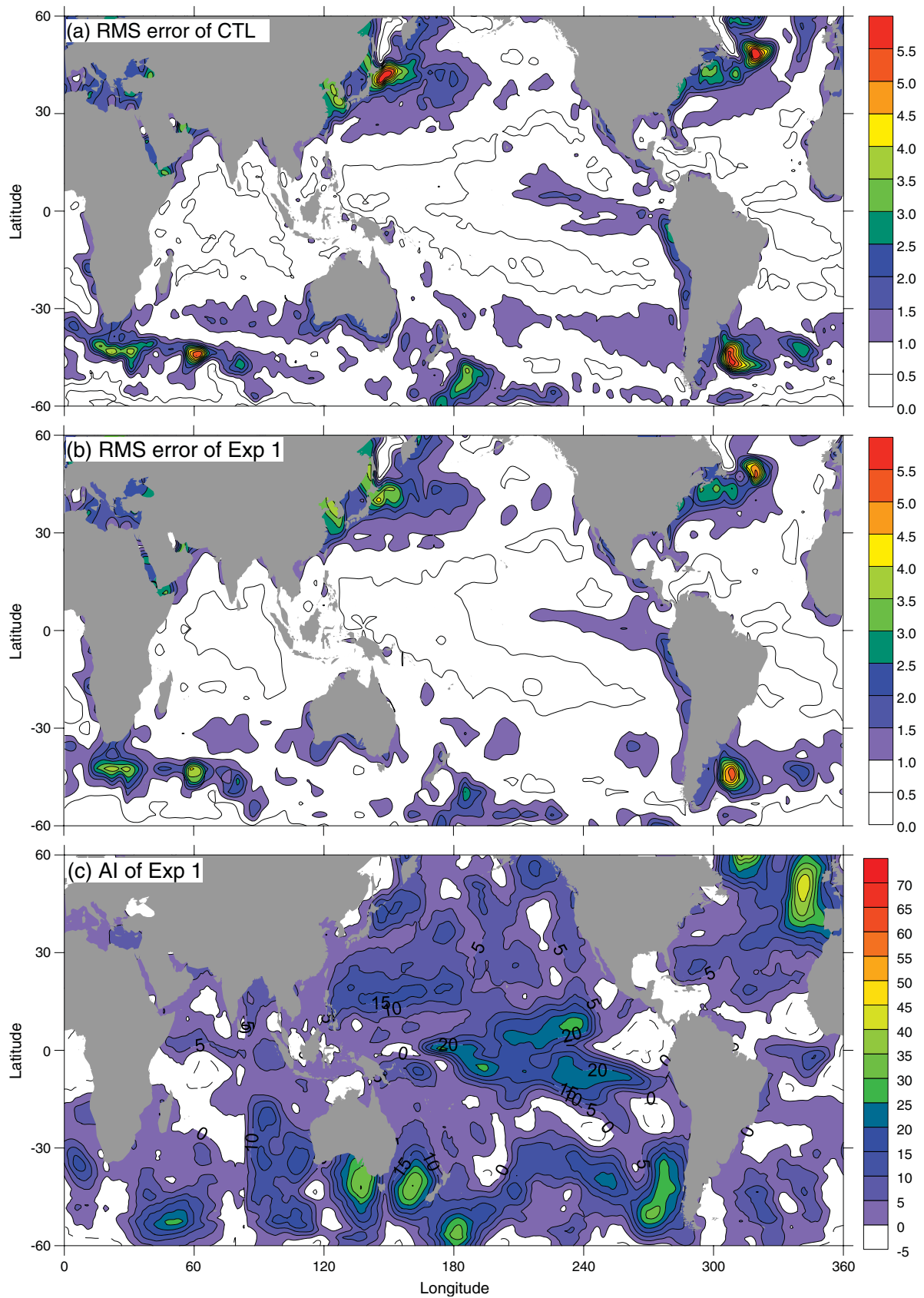


Fig. 8 Spatial distribution of RMS errors in SST for the two base experiments. The contour interval for the RMS error is 0.5°C , and for AI, 5%. The colored regions are for RMS errors greater than 1°C and for the positive AI

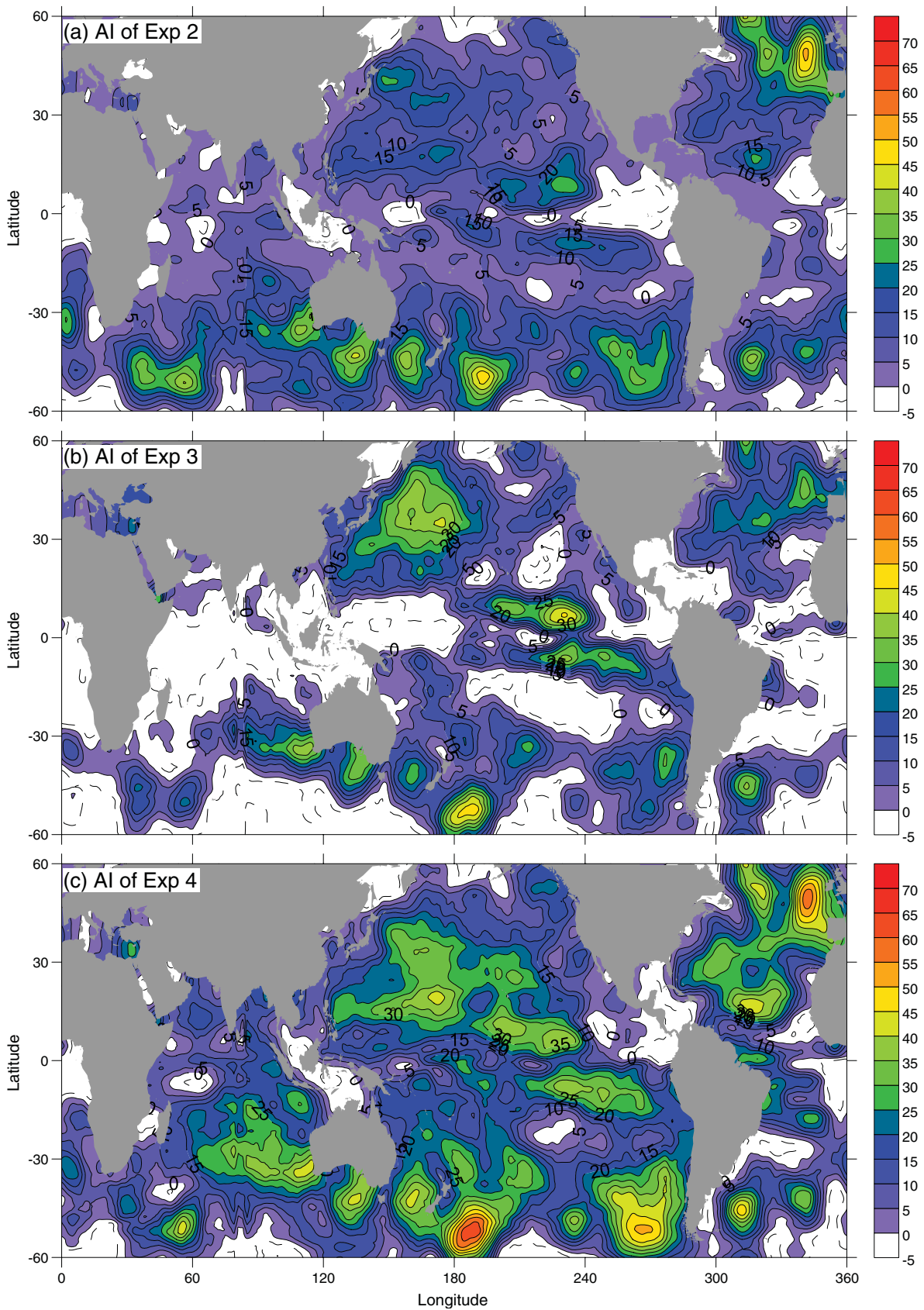


Fig. 9 Spatial distribution of AI for sensitivity experiments. The contour interval is 5%, and the *colored regions* are for the positive AI

perturbation amplitude (Exps 2 and 3) only causes a great difference in the beginning period of the ODA. The optimal ensemble inflation of 5% improves the performance of Argo data assimilation and gives the best result among all the experiments carried out in this study.

Further comparison with satellite SST is carried out to confirm the results from the comparison with the GTSP profiles. The performance of Exp 1 in the second half of 2008 is, however, not as good as in the first half of the year. The experiments of different perturbation layers and amplitudes (Exps 1–3) indicate that perturbing all layers of the ocean is much better than only perturbing the upper ocean and that the perturbation amplitude is important for the beginning period of ODA. The results of Exp 4 with an optimal inflation factor of 5% can indeed improve the assimilation performance.

Only the sea temperature in OGCM is perturbed in the whole water column according to its variance; and then a finite temperature ensemble spread will be generated directly. Because of the existence of the relationship among model variables, the ensemble spreads of the unperturbed variables are also generated by the adjustment of the model itself through numerical integration. This perturbation method is easy to implement and the induced ensemble spread can keep well the dynamical balance inside the model. But comparing to the model uncertainties, the induced ensemble spread may be smaller in sometime. As the result, the EAKF analysis process becomes inaccurate and the ensemble inflation is necessary for a better assimilation performance. More efforts on improving the perturbation method should be attempted on the view of dynamics in the future.

Since high costs of computation time and storage are needed to determine the optimal inflation factor in this study, a more efficient way should be sought in the future. In addition, other methods for ensemble inflation, such as the adaptive covariance inflation error correction algorithm, should be tested further. We plan to include in this EAKF module many other kinds of observations, including satellite SST, sea-surface height from satellite altimeter, and other in situ temperature/salinity profiles, for more realistic applications.

Acknowledgment The work was jointly supported by the Project of the National Basic Research Program of China under contract No. 2007CB816002 and a special fund for the Fundamental Scientific Research under contract No. 2008 G08.

Open Access This article is distributed under the terms of the Creative Commons Attribution Noncommercial License which permits any noncommercial use, distribution, and reproduction in any medium, provided the original author(s) and source are credited.

References

- Anderson JL (2001) An ensemble adjustment Kalman filter for data assimilation. *Mon Weather Rev* 129:2884–2903
- Anderson JL (2003) A local least squares framework for ensemble filtering. *Mon Weather Rev* 131:634–642
- Anderson JL (2007) An adaptive covariance inflation error correction algorithm for ensemble filters. *Tellus* 59A:210–224
- Anderson JL, Hoar T, Raeder K et al (2009) The data assimilation research testbed: a community data assimilation facility. *Bull Amer Meteor Soc* 90:1283–1296
- Bishop CH, Etherton BJ, Majumdar S (2001) Adaptive sampling with the ensemble transform Kalman filter, part I: theoretical aspects. *Mon Weather Rev* 129:420–436
- Carton JA, Chepurin G, Cao X et al (2000a) A simple ocean data assimilation analysis of the global upper ocean 1950–1995, part 1: methodology. *J Phys Oceanogr* 30:294–309
- Carton JA, Chepurin G, Cao X et al (2000b) A simple ocean data assimilation analysis of the global upper ocean 1950–1995 part 2: results. *J Phys Oceanogr* 30:311–326
- Chepurin G, Carton JA, Dee DP (2005) Forecast model bias correction in ocean data assimilation. *Mon Weather Rev* 133:1328–1342
- Courtier P, Derber J, Errico R et al (1993) Important literature on the use of adjoint, variational methods and the Kalman filter in meteorology. *Tellus* 45A:342–357
- ETOP5 (1986) 5'×5' topography and elevation. Marine Geology and Geophysics Division, National Geophysical Data Center. (Available from National Geophysical Data Center, NOAA, Code E/GC3, Boulder, CO 80303)
- Evensen G (1994) Sequential data assimilation with a nonlinear quasi-geotropic model using Monte Carlo methods to forecast error statistics. *J Geophys Res* 99(10):143–162
- Evensen G (2003) The ensemble Kalman filter: theoretical formulation and practical implementation. *Ocean Dyn* 53:343–367
- Evensen G (2004) Sampling strategies and square root analysis schemes for the EnKF with correction. *Ocean Dyn* 54:539–560
- Ezer T, Mellor GL (1994) Continuous assimilation of GEOSAT altimeter data into a three dimensional primitive equation Gulf Stream model. *J Phys Oceanogr* 24:832–847
- Ezer T, Mellor GL (1997) Data assimilation experiments in the Gulf Stream region: how useful are satellite-derived surface data for nowcasting and the subsurface fields? *J Atmos Oceanic Technol* 14:1379–1391
- Griffies SM, Harrison MJ, Pacanowski RC et al (2007) Ocean modelling with MOM. *Clivar Exchanges* 12(3):3–5
- Hamill TM, Whitaker JS, Snyder C (2001) Distance-dependent filtering of background error covariance estimates in an ensemble Kalman filter. *Mon Weather Rev* 129:2776–2790
- Houtekamer PL, Mitchell HL (1998) Data assimilation using an ensemble Kalman filter technique. *Mon Weather Rev* 124:796–811
- Kalman R (1960) A new approach to linear filtering and prediction problems. *Transact ASME–J Basic Eng* 82(D):35–45
- Kalman R, Bucy R (1961) New results in linear filtering and prediction theory. *Transact ASME–J Basic Eng* 82(D):95–109
- Kalnay E, Kanamitsu M, Kistler R et al (1996) The NCEP/NCAR 40-year reanalysis project. *Bull Amer Meteor Soc* 77:437–470
- Karspeck A, Anderson JL (2007) Experimental implementation of an ensemble adjustment filter for an intermediate ENSO model. *J Climate* 20:4638–4658
- Levitus S, Boyer TP (1994) World Ocean Atlas 1994: temperature and salinity. US Department of Commerce, Washington, D.C
- Mellor GL, Ezer T (1991) A Gulf Stream model and an altimetry assimilation scheme. *J Geophys Res* 96:8779–8795
- Pham DT (2001) Stochastic methods for sequential data assimilation in strongly non-linear system. *Mon Weather Rev* 129:1194–1207
- Qiao F, Yuan Y, Yang Y et al (2004) Wave-induced mixing in the upper ocean: distribution and application in a global ocean circulation model. *Geophys Res Lett* 31:L11303. doi:10.1029/2004GL019824

- Shu Q, Qiao F, Song Z et al (2011) Improvement of MOM4 by including the surface wave-induced vertical mixing. Submitted to Ocean Modelling (in press)
- Tippett MK, Anderson JL, Bishop CH et al (2003) Ensemble square-root filters. *Mon Weather Rev* 131:1485–1490
- Whitaker JS, Hamill TM (2002) Ensemble data assimilation without perturbed observations. *Mon Weather Rev* 130:1913–1924
- Winton M (2000) A reformulated three-layer sea ice model. *J Atmos Ocean Technol* 17:525–531
- WOCE/CLIVAR (2002) WOCE/CLIVAR Working Group on Ocean Model Development. Report of the Third Session. World Climate Research Programme, Informal Rep. No. 14/2002
- Yin X, Oey LY (2007) Bred-ensemble ocean forecast during Katrina: loop current and ring. *Ocean Model* 17(4):300–326
- Yin X, Qiao F, Yang Y (2010a) Ensemble adjustment Kalman filter study for Argo data. *Chin J Oceanol Limnol* 28(3):626–635
- Yin X, Qiao F, Xia C et al (2010b) Reconstruction of eddies by assimilating satellite altimeter data into Princeton Ocean Model. *Acta Oceanol Sin* 29(1):1–11
- Zhang S, Anderson JL (2003) Impact of spatially and temporally varying estimates of error covariance on assimilation in a simple atmospheric model. *Tellus* 55A(2):126–147
- Zhang S, Harrison MJ, Wittenberg AT et al (2005) Initialization of an ENSO forecast system using a parallelized ensemble filter. *Mon Weather Rev* 133:3176–3201
- Zhang S, Harrison MJ, Rosati A et al (2007) System design and evaluation of coupled ensemble data assimilation for global oceanic climate studies. *Mon Weather Rev* 135:3541–3564
- Zhang S, Rosati A (2010) An inflated ensemble filter for ocean data assimilation with a biased coupled GCM. *Mon Wea Rev*. doi:10.1175/2010MWR3326.1